

PCCP

Accepted Manuscript



This is an *Accepted Manuscript*, which has been through the Royal Society of Chemistry peer review process and has been accepted for publication.

Accepted Manuscripts are published online shortly after acceptance, before technical editing, formatting and proof reading. Using this free service, authors can make their results available to the community, in citable form, before we publish the edited article. We will replace this *Accepted Manuscript* with the edited and formatted *Advance Article* as soon as it is available.

You can find more information about *Accepted Manuscripts* in the [Information for Authors](#).

Please note that technical editing may introduce minor changes to the text and/or graphics, which may alter content. The journal's standard [Terms & Conditions](#) and the [Ethical guidelines](#) still apply. In no event shall the Royal Society of Chemistry be held responsible for any errors or omissions in this *Accepted Manuscript* or any consequences arising from the use of any information it contains.

ARTICLE

FTO-free counter electrodes for dye-sensitized solar cells using carbon nanosheets from a polymeric carbon source

Cite this: DOI: 10.1039/x0xx00000x

Zico Alaia Akbar,^{a§} Jae-Seon Lee,^{b,c§} Jinhyeon Kang,^a Han-Ik Joh,^bReceived 00th January 2014,
Accepted 00th January 2014Sungho Lee,^{b,c*} Sung-Yeon Jang^{a*}

DOI: 10.1039/x0xx00000x

www.rsc.org/

Highly conductive carbon nanosheets (CNSs) are fabricated using a polymeric carbon source and subsequently applied as the counter electrodes (CNS-CEs) for dye-sensitized solar cells (DSSCs). The CNSs have a similar structure to multilayered graphene, and their high electrical conductivity and electrocatalytic activity enables them to have a dual-function as both CEs and charge supporting electrodes. CNSs form a unique CE material that functions successfully while being metal- and fluorine doped tin oxide (FTO)-free and allowing DSSCs to achieve ~ 5% power conversion efficiency. The chemical structure, electrical properties, electrocatalytic activity, and work function of the CNS-CEs prepared by various conditions of carbonization are investigated, and their effects on the performance of the corresponding DSSCs are discussed. Carbonization temperature is shown to have influenced the size of graphitic domains and the presence of heteroatoms and functional groups in CNS-CEs. The change in graphitic domain size has a marginal influence on the work function of the CNS-CEs and the overpotential for the reduction of the redox couples (I/I_3^-). However, the electrical conductivity of CNS-CEs and charge transfer resistance at CE/electrolyte interfaces in the DSSCs are considerably influenced by the carbonization condition. Our study shows that CNSs serve as an efficient, FTO-free CE material for DSSCs, and they are an appropriate material with which the effects of the chemical/physical properties of graphene-based materials on the electrode performance for various electrochemical devices may be studied.

Introduction

Dye-sensitized solar cells (DSSCs) have attracted many researchers as emerging energy conversion devices due to their low production cost and relatively high conversion efficiency.¹ A recent achievement in power conversion efficiency (PCE) of up to 13.1 %² is high enough to allow for the opportunity of commercialization, if the cost and mass production process meet the product's standard requirements. A typical DSSC consists of a dye-sensitized nanocrystalline TiO₂ photoelectrode that sits in a transparent conducting electrode (TCO), such as fluorine doped tin oxide, (FTO) coated glass, an electrolyte containing redox couples (for example I^-/I_3^-), and a counter electrode (CE). Although less studied compared to the other components in DSSCs, CEs play an essential role in regulating device performance by electrocatalytically reducing the redox couples that are oxidized after dye regeneration. A good CE for DSSCs (DSSC-CEs) should have a low charge transfer resistance at the CE/electrolyte interface; in other words, a high electrocatalytic reaction rate and low overpotentials for the redox reaction. Low sheet resistance (high electrical conductivity) is another important criterion in providing sufficient charge for the electrochemical

reduction. Chemical stability of the CE and a low production cost are other practical requirements for commercialization of DSSCs.

Crystalline Pt prepared through thermal pyrolysis or sputtering process coated on FTO has been a conventional material for the CEs. In the typical Pt/FTO based CEs, Pt showed the sufficient electrocatalytic activity required to produce the requisite redox reactions, and the supporting FTO/glass fulfills the high conductivity requirements for a given electron supply. However, both materials are too expensive to use in the commercial manufacture of DSSCs, thus seeking lower-cost alternative materials has been the principal research direction for DSSC-CE. For the catalytic materials, various types of alternative materials such as active carbon,^{3, 4} carbon nanotubes (CNTs),^{5, 6} graphene,⁷⁻⁹ conducting polymers,^{10, 11} and transition metals^{12, 13} have been studied and show promising results. FTO provides the high electrical conductivity required to supply effectively the necessary amount of charge for the redox reaction to the Pt catalyst. Reduction of the efficiency of the charge supply can decrease the redox reaction rate and correspondingly impairs device performance. Although FTO is one of the most efficient charge supporting electrodes due to its high conductivity and rough surface, the high cost of Pt/FTO-based CEs is approximately 40 % of the

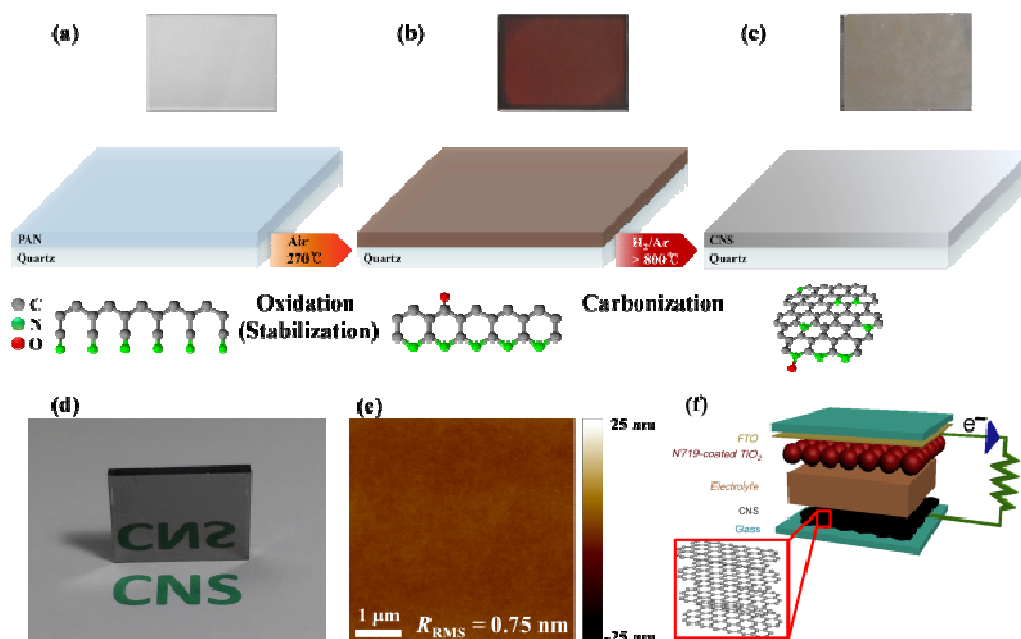


Fig. 1. Schematic illustration of CNS-CE fabrication process (a – c), the photo image (d) and AFM image of CNS-CEs (e), and the structure of DSSC-CNSs (f) used in this study. The images (d and e) in this Fig. were obtained from sample CNS-1000.

total cell cost, presenting an obstacle in the commercialization of DSSC.¹⁴

In order to replace FTO in CEs, the alternative materials should have sufficient electrical conductivity and catalytic activity simultaneously. This stringent requirement limited the choice of materials, and several FTO-free CEs have been suggested including other metal oxide based TCO materials,¹⁴ polymers,¹⁵⁻¹⁷ carbon materials,¹⁸⁻²⁰ and metals such as stainless steel.²¹ Among them, carbon materials have advantages in terms of abundance and cost, while variety of synthetic methods available. Although the electrical conductivity of carbon-based materials is not as high as that of metals or FTO, recently developed graphene-based materials (GBMs) demonstrate promisingly high conductivity.²²⁻²⁴ GBMs have been shown to have a range of conductivity that is dependent on the method of synthesis (chemical vapor deposition (CVD),²⁴ wet-chemical synthesis,²⁵ and epitaxial growth).²⁶ Variability of the electrical conductivity in GBMs is expressed as changes in the amount of graphite and number of defects. Understanding the electrical and electrochemical properties of GBMs in terms of their chemical structures and method of synthesis is an important study in developing low-cost, FTO-free carbon-based CEs.

In this study, novel carbon nanosheets (CNSs) were fabricated by a unique catalyst-free pyrolysis process using a polymer precursor, polyacrylonitrile (PAN). The preparation method resembles the fabrication process that produces conventional carbon fibers (oxidation followed by carbonization), and the resulting CNSs were similar to multilayered graphene. The evolution of chemical structures with respect to carbonization conditions and their corresponding influence on electrical conductivity, electrocatalytic activity for the redox media (I_3^-/I^-), and work function were

investigated. It was observed that carbonization temperature influences the size of graphite domains and the portion of heteroatoms and functional groups in CNS-CEs, which in turn influence the electrical conductivity of CNS-CEs and the charge transfer resistance at CNS-CE/electrolyte interfaces of DSSCs. The work function and overpotential for the redox reaction changed marginally. Optimized CNS-CEs display sufficient electrical conductivity and electrocatalytic activity and function successfully as metal- and FTO-free CEs allowing DSSCs to achieve a power conversion efficiency (PCE) of ~ 5%.

Experimental

Preparation of CNS-CEs

To fabricate PAN-based carbon nanosheets (CNS) for counter electrode, polyacrylonitrile (PAN) (Aldrich, average MW = 150,000 g/mol) solutions with the concentration of 5–8 wt% were prepared by dissolving PAN in N, N-dimethylformamide (DMF) (Fisher, HPLC grade). The PAN solutions were spin-coated directly on bare quartz. The spun-coated PAN films were stabilized at 270 °C for 2 h under air followed by carbonization at 800 - 1200 °C in H₂/Ar atmosphere.

Fabrication of DSSCs

A commercial TiO₂ paste, that consists of 20 nm sized of TiO₂ nanoparticle, was used to produce TiO₂ transparent layer. Approximately 9 μm thickness of transparent TiO₂ paste was deposited onto clean FTO glass by doctor blade technique. Adhesive tape (Scotch, 50 μm) was used in order to control the TiO₂ layer

thickness. The transparent layer was then heated at 125 °C for 5 minutes. Following this, 3 μm of TiO₂ paste containing 500 nm sized particles was coated onto the transparent 20 nm TiO₂ layer. The photoelectrodes were heated again to 125 °C for 5 minutes before furthering annealing gradually from 300 °C to 500 °C for 1 hour 20 minutes using a programmable furnace. The annealed photoelectrodes were treated with 0.2 M TiCl₄ solution for 30 minutes at 70 °C. After treatment with TiCl₄, the photoelectrodes were annealed again at 500 °C for 30 minutes. The N719 dye, Ru(dcbpy)₂(NCS)₂(dcbpy = 2,2-bipyridyl-4,4-dicarboxylato); was used to sensitize the TiO₂ photoelectrodes. The photoelectrodes were then immersed for about 18 hours in a 0.3 mM dye solution containing a mixture of acetonitrile (ACN) and tert-butyl alcohol (1:1) (v/v) and dried at room temperature. The as-prepared CNSs on quartz glasses were used as the counter electrodes. The CNS-CEs were drilled using a micro-drill and consecutively cleaned with ethanol for 10 minutes. The counter electrode and the prepared photoelectrodes were then assembled together, they are separated by a 25 μm thick surlyn between two electrodes, to form a sandwich-type configuration. Then a conventional organic electrolyte, 0.65 M (BMII), 0.1 M guanidiumthiocyanate (GuSCN), 0.03 M I₂, and 0.5 M 4-terbutylpyridine in acetonitrile/valeronitrile (85:15, vol%), was introduced into the cell via the drilled holes. Finally, the holes were sealed with a thermal adhesive film and a cover glass.

Characterizations

A Raman spectrometer (Horiba, LabRAM HR UV-Visible-NIR) with laser excitation wavelength of 514.5 nm and a power of 16mW was used to observe graphitic structural development of CNS. To investigate chemical bonds and relative content of elements of CNS, X-ray photoelectron spectra were obtained (Thermo Scientific, K-alpha) using monochromated Al Kα (1486.6 eV) X-rays below a pressure of 3×10⁻⁷ Torr. An atomic force microscope (AFM, Veeco, SPM Dimension 3100 with Nanoscope IIIA controller) in tapping mode was employed to investigate surface morphology and thickness of CNS. To evaluate electrical conductivity, sheet resistance was measured by four-point probes (FPP-RS8, Dasol Eng., Korea). Ultraviolet photoelectron spectroscopy (UPS) was performed using Kratos AXIS Ultra DLD to confirm work function of CNS with He I (21.2 eV). The scanning electron microscopy (SEM) measurements of CNSs were conducted on a LEO-1530 microscope (Germany). Cyclic Voltammetry was run using Ag/Ag⁺ (AgNO₃ 10 mM), 0.1 M LiClO₄, in acetonitrile as the reference electrode, and Pt plate as counter electrode respectively. The electrolyte consists of 0.1 M LiClO₄, 5mM LiI, and 0.5 mM I₂. The active area was set to be ~1.08 Cm². Current density–voltage (*J*-*V*) characteristics of the DSSCs were obtained under 1 sun illumination (light intensity was adjusted using a Si Solar Cell equipped with a BK5 filter for approximating AM 1.5 G 100 mW.cm⁻² light radiation intensity) with a Newport (USA) solar simulator (450W Xe source) and a Keithley 2400 source meter. The area of the as-fabricated photoactive layers was ranged at 0.25 ~ 0.35 cm² and the cell performance was measured using black metal mask (area of 0.175 cm²). EIS measurement were done using an impedance analyzer (Solatron 1260) at an open circuit condition under 1.5 G

light illumination with frequency range of 0.1 to 10⁵ Hz. EIS data obtained was then fitted using Z-Plot Software to gain each impedance parameter.

Results and discussion

The CNSs were prepared by a catalyst-free pyrolysis process that is similar to the conventional carbon fiber fabrication process, using a polymer precursor, PAN, as a carbon source (Fig. 1). PAN is a popular polymer precursor for carbon fibers because it has excellent productivity due to its high conversion efficiency to carbon. The resulting carbon fibers contained an improved portion of graphitic structures, which provide enhanced performance. A solution of PAN in dimethylformamide (DMF) was spin-coated onto a quartz plate (Fig. 1a), and then the resultant films were oxidized at 270 °C for 2 h in an air atmosphere to induce the formation of a ladder-like structure by cyclization of the polymer chain (Fig. 1b and Fig. S1 in supplementary information, SI). The films were then carbonized at a range of temperatures (800 ~ 1200 °C) under a H₂/Ar mixture to yield CNSs (Fig. 1c and Fig. S1). The resulting CNSs were black films with shiny surfaces indicating high flatness (Fig. 1d). The surface roughness of the films was analyzed by atomic force microscopy (AFM). The root mean square roughness (*R*_{RMS}) value of a CNS films prepared at the carbonization temperature 1000 °C was ~0.75 nm (Fig. 1e) which is similar to that of the polymer precursor films (data not shown). The *R*_{RMS} values of all CNS films were ranged 0.6–0.8 nm as shown in Fig. S2. This result indicates that the

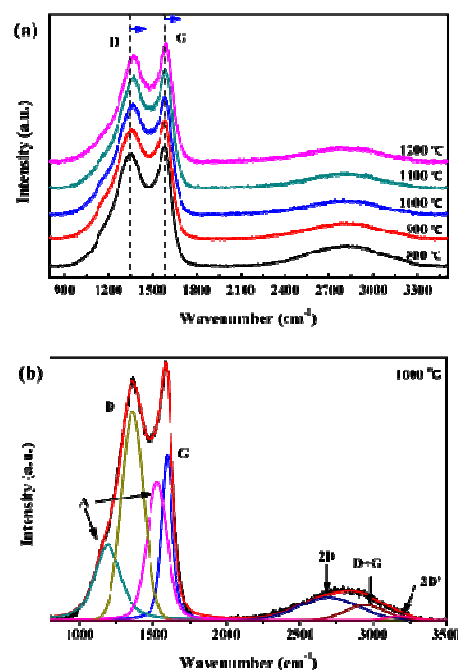


Fig. 2. Raman spectra of CNSs prepared at a range of carbonization temperatures; pristine Raman spectra (a) and the deconvoluted version of a spectrum (CNS-1000) obtained using a mixed Gaussian–Lorentzian function (b). The concentration of PAN solution in DMF for spin-coating was 8%. The peaks A in (b) were originated from the amorphous portion of CNSs.

quality of PAN films is maintained during the oxidation followed by carbonization process. Our synthesis strategy is also similar to that used in the preparation of multilayered graphene using a polymeric carbon source. However, this work demonstrates uniqueness in our process as it is done without using a metal catalyst.

Raman spectra in Fig. 2 show evidence of the graphitic structures in the CNSs prepared at a range of carbonization temperatures. All the CNS films exhibited two principal peaks (D peak at $\sim 1350\text{ cm}^{-1}$ and G peak at $\sim 1600\text{ cm}^{-1}$) and a broad peak at $\sim 2800\text{ cm}^{-1}$ (convolution of 2D, D+G and 2D'), which are commonly observed in sp^2 bonded carbon materials including graphene. The deconvoluted Raman spectra of a representative CNS (CNS-1000, thereafter, the numbers following CNS indicate their carbonization temperatures in centigrade), were shown in Fig. 2b. The presence of an amorphous portion in the spectral region between 1100 cm^{-1} to 1600 cm^{-1} revealed that the CNSs are not composed of a perfect sp^2 network.²⁷ Notably, the Raman spectra of the CNSs in Fig. 2 were similar to those of chemically prepared graphene, which contain some portion of defects and amorphous area.²⁸ The sharp D and G peaks of CNSs were blue-shift with increasing carbonization temperature, while the amorphous peaks (denoted as A in Fig. 2b) were diminished (also refer Fig. S3). These results indicate an increase of sp^2 carbon networks and/or enhancement of the graphitic structure at higher carbonization temperature.²⁹ The intensity ratio of the D and G peaks (I_D/I_G) is a typical criterion used to determine the graphitic domain size (L_a) and can be calculated using an empirical equation; $L_a\text{ (nm)} = 4.4(I_D/I_G)^{-1}$, according to the previous works by Knight et al.³⁰ The enlarged graphitic domain sizes of CNSs carbonized at higher temperatures ($> 1000\text{ }^\circ\text{C}$) were confirmed by the increase in corresponding L_a values. The Raman peak positions, intensities, and L_a values of the CNSs prepared at various carbonization temperatures are summarized at Table 1.

The as-prepared CNSs were used directly as CEs for the DSSCs. A Ru complex sensitizer (N719, Solaronix) attached TiO_2 nanoparticles was used as the photoelectrode, and an organic electrolyte containing conventional I^-/I_3^- redox species was filled. The structure of the DSSCs using the CNS-CEs (DSSC-CNSs) is shown in Fig. 1f. The current density-voltage (J - V) characteristics of the DSSC-CNSs under one sun illumination (AM 1.5G, 100 mWcm^{-2}) were shown in Fig. 3a, and the detailed cell parameters are summarized at Table 2.

Table 1. The peak positions and intensity ratio of D and G peaks from Raman spectra, and the calculated graphitic domain size (L_a) of CNSs (the numbers after CNSs indicate their carbonization temperatures at centigrade). The L_a values were calculated using the relation; $L_a\text{ (nm)} = 4.4(I_D/I_G)^{-1}$.

CNS samples	D (cm^{-1})	G (cm^{-1})	I_D/I_G	L_a (nm)
CNS-800	1348.2	1594.1	1.41	3.12
CNS-900	1353.0	1594.5	1.31	3.36
CNS-1000	1360.0	1594.8	1.27	3.46
CNS-1100	1361.8	1596.6	1.14	3.85
CNS-1200	1365.7	1598.0	1.04	4.07

Fig. 3b shows the variations of cell parameters after analyzing more than 15 cells fabricated using CNS-CE that is prepared under different carbonization conditions. The PCEs of the DSSC-CNSs varied according to the types of CNSs. The DSSC-CNSs using the CNSs prepared at carbonization temperatures higher than $1000\text{ }^\circ\text{C}$ displayed improved performance, reaching a PCE of $\sim 5\%$. The average PCE of DSSC-CNSs using the CNS-1200 was 4.74% (open circuit voltage (V_{OC}) = 680 mV , short circuit current (J_{SC}) = 15.62 mA , fill factor (FF) = 45%), which is $\sim 35\%$ higher than that of cells using CNS-900 (PCE = 3.52% ; V_{OC} = 670 mV , J_{SC} = 16.16 mA , FF = 33%). This is an impressive performance for a CE, when taking into account the fact that any additional charge supporting electrodes such as FTO or metal plates were not used. In conventional DSSCs, charge supporting electrodes such as FTO are regularly used owing to their high conductivities with respect to supplying or collection of electrons, thus the limited charge transport capability of CEs can be compensated. However, using FTO significantly raises the cost of DSSCs. As shown in Fig. 3b, the major distinction of the cell performance was governed by a change in FF of the cells (except the far reduced J_{SC} at CNS-800), whereas V_{OC} and J_{SC} are relatively similar in all DSSC-CNSs and are also comparable to those of other reported DSSCs using carbon based CEs with the same sensitizer and electrolyte.

Because FF of DSSCs is directly related to the internal series resistance (R_s) of the cells, the R_s values of the DSSC-CNSs were analyzed using electrochemical impedance spectroscopy (EIS).³¹

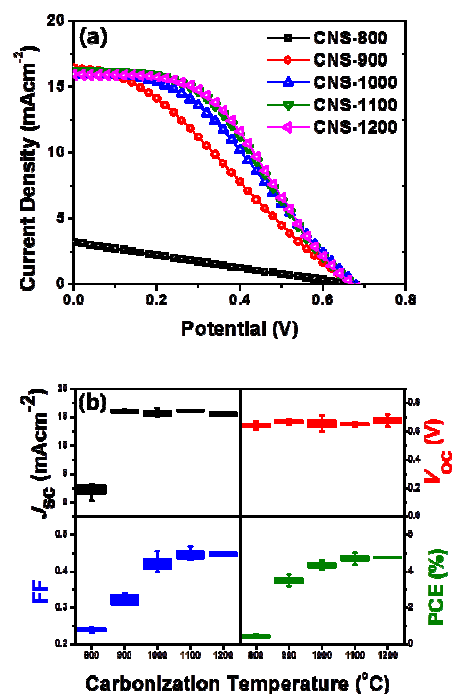


Fig. 3. Current density-voltage (J - V) characteristics of various DSSC-CNSs (a) and the plots of the cell parameters obtained from various DSSC-CNSs (b). The numbers of cells used to obtain the range of variation were 10 for each type of CNS-CE.

Table 2. The cell parameters obtained from J - V curves analysis of DSSC-CNSs. PCE value from champion cells are given in the bracket.

CNS-CEs	V_{oc} (V)	J_{sc} (mA cm ⁻²)	FF	PCE (%)	R_s (Ω cm ⁻²)	R_{CT} (Ω cm ⁻²)
CNS-800	0.66	3.16	0.24	0.51 (0.52)	1262	762
CNS-900	0.66	16.49	0.31	3.37 (3.67)	248	206
CNS-1000	0.66	16.03	0.40	4.22 (4.55)	122	84
CNS-1100	0.66	16.17	0.44	4.66 (4.94)	101	33
CNS-1200	0.66	16.23	0.45	4.75 (4.75)	104	34

Fig. 4a shows the Nyquist plots of DSSC-CNSs measured at V_{oc} condition under one sun illumination. The high frequency (leftmost semicircle in Fig. 4a) indicates the electrochemical charge transfer resistance at the CE/electrolyte interface (R_{CT}) while the semicircles at mid-frequency and low frequency indicate impedance by transport and recombination competition at the TiO_2 /dye/electrolyte interface, as well as impedance by Nernst diffusion in the I^-/I_3^- redox species in the electrolyte (refer to the inset graph of Fig. 4a).³ The values of R_s and R_{CT} of DSSC-CNSs can be obtained from the real component (Z') values;^{32-35]} the R_{CT} was differentiated using the equivalent circuit diagram in the inset of Fig. 4a. Both the R_s and R_{CT} values of the DSSC-CNSs were significantly reduced when the CNSs were prepared at temperatures above 1000 °C. The R_{CT} of the DSSC-CNSs using CNS-1200 was 6-fold lower (34 Ω cm²) than that of CNS-900 (206 Ω cm²) in accordance to the FF of the DSSC-CNSs. The extraordinarily large R_s value of the cells using CNS-800 indicates that a negligible amount of charge transfer occurs at the CNS-800/electrolytes interfaces, which are responsible for the low J_{sc} and FF of the corresponding DSSCs. The characteristic peaks in the Bode plots (Fig. 4b) were shifted to a higher frequency as the carbonization temperature was increased, confirming the enhanced charge transfer.³⁶ The charge transfer behavior at the CNS-CE/electrolyte interface regarding the reduction of I_3^- to I^- seems to vary depending on the types of CNSs. Further characterization results on the electrocatalytic activity and chemical structures of various CNS-CEs and the discussion on the factors affecting charge transfer will be discussed in the following sections.

In order to further investigate the electrocatalytic activity of CNS-CEs on the redox reaction of the I^-/I_3^- couples, cyclic voltammetry (CV) analysis was performed (Fig. 5). In the CV analysis, the CNS-CEs were used as the working electrodes in a CH_3CN solution containing 0.1 M $LiClO_4$, 5 mM LiI , and 0.5 mM I_2 . The deposition area for all the CNS-CEs was ~ 1.09 cm². The redox pair at the more positive potentials is due to reaction $I_3^- + 2e^- = 3I^-$, while the redox pair at the more negative potentials is the redox pair of $3I_2 + 2e^- = 2I_3^-$.^{9,37} The left pair of peaks, which show the I^-/I_3^- redox process, is of interest for the performance of the CE. The peak-to-peak separation (E_{pp}) of the left pairs can elucidate redox reaction kinetics at the CEs. The E_{pp} and the peak positions of all the CNS-CEs were almost identical regardless of the carbonization conditions (~ 0.95 V), which is somewhat similar to that of the chemically prepared graphene/FTO based CEs. However, the E_{pp} was wider than regular

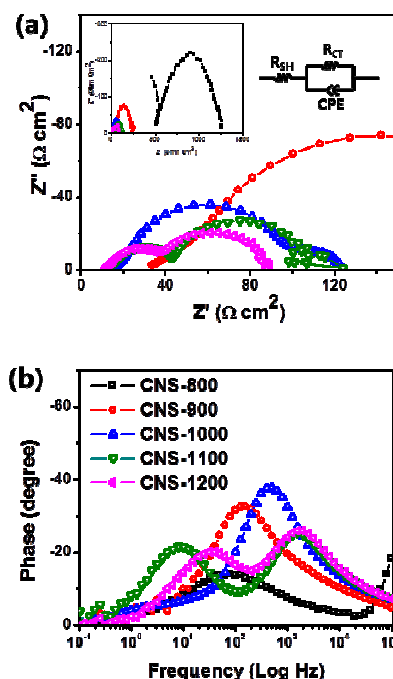


Fig. 4. EIS analysis results of the DSSC-CNSs; (a) Nyquist plots and (b) Bode plots. The circuit diagram used for the simulation of the CE/electrolyte interface (R_{CT}) is depicted in the inset of (a).

Pt/FTO based CEs (~ 0.3 V, also refer the inset graph in the inset of Fig. 5).^{8,38}

This result implies that the overpotentials for the electrocatalytic reduction of I_3^- are similar regardless of the types of CNSs, although they are higher than that of Pt/FTO based CEs. However, the peak exchange current (I_p) values, which are closely related to the extent of redox reaction that takes place on the CEs, significantly increases in CNS-CEs prepared above 1000 °C. This indicates that a great number of net redox reactions occurred forming the CNSs prepared at higher temperatures. It is important to note that the specific

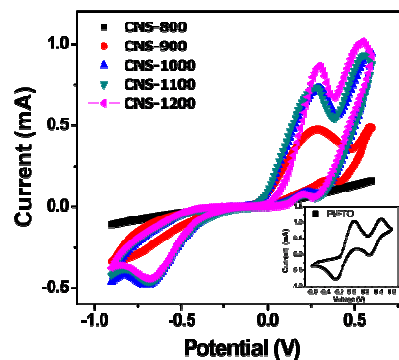


Fig. 5. Cyclic voltammetry (CV) analysis results of CNS-CEs carbonized at various temperatures. The inset graph is a CV result of a regular Pt/FTO based CE.

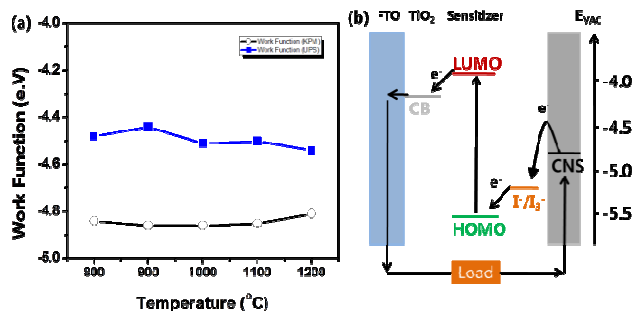


Fig. 6. Work function (WF) values of the CNS-CEs measured by KPM and UPS (a) and the diagram for working principle of DSSCs (b).

surface areas of the GNS-CEs were almost identical (also refer to AFM images in Fig. S2) and so are the E_{pp} values, the improved electrocatalysis, which in turn directly reflects cell performance, has been attributed to the changes in other properties of CNSs.

The work function (WF) of the CNS-CEs was measured using Kelvin probe microscopy (KPM) and ultraviolet photoelectron spectroscopy (UPS) in order to elucidate the origin of the same overpotentials for the redox reaction (Fig. 6 and Fig. S4). In the DSSCs using graphene based CE, the WF values of the graphene often altered their electrocatalytic activity, in addition to the V_{OC} , series resistance, and cell performance.³⁹ The WF values of our CNS-CEs were almost identical regardless of the types of CNSs. The WFs measured by UPS ranged from 4.44 ~ 4.54 eV, while those measured by KPM ranged 4.81 ~ 4.86 eV (Fig. 6). Our WF values were similar to reported values of graphene/FTO based CE [12]. The similar WF values were in accordance with the almost identical overpotentials measured in all types of CNS-CEs found in the CV analysis (E_{pp} values in Fig. 5). The V_{OC} values of our DSSC-CNSs were similar to those reported on DSSCs using graphene/FTO CE.³⁹ Kang et al. reported that tuning of WF in graphene/FTO CE could be done by doping with nitric acid.³⁹ In that report, the WFs of the CE varied from 4.52 eV to 5.31 eV, measured by UPS; indicating enhanced electrocatalytic activity and reduced R_s . Upon increasing WF, the V_{OC} values increased up to ~0.1 V, and the optimized PCE reached to 3.2%.³⁹ Notably, in the case of our CNS-CEs, the PCEs reached to ~ 5 % without using FTO.

The electrical properties of the CNS-CEs were measured using a 4-point probe configuration. The electrical conductivities and surface sheet resistances of the CNS-CEs are shown in Fig. 7. Sheet resistance has shown to be reduced as the carbonization temperature is increased; there was also abrupt reduction up to CNS-1000 followed by a gradual decrease thereafter. This reduced sheet resistance in CNS-CEs prepared at higher carbonization temperatures is in good agreement with the enlarged crystal domain sizes that are calculated based on Raman spectra (Table 1). However, more detailed chemical structure evolution with respect to the carbonization temperature was investigated to further elucidate the relationship between the chemical structure and the resulting electrical properties.

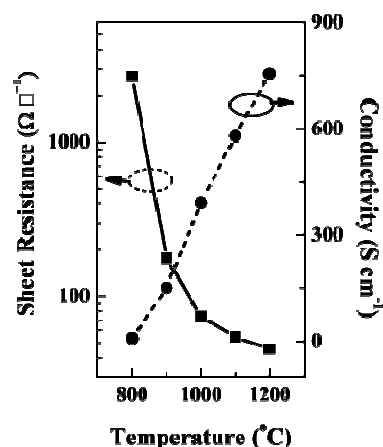


Fig. 7. Electrical conductivity and surface sheet resistance of various types of CNS-CEs carbonized at different temperatures.

The chemical composition of the various CNSs was analyzed using X-ray photoelectron spectroscopy (XPS), and the resulting XPS spectra are shown in Fig. S5. Fig. 8 displays the compositions of functional groups and the atomic ratio (for three major elements C, N, and O) of various CNSs. As the carbonization temperature increases, the atomic ratio of C increases and those of heteroatoms such as N and O decreases (Table S1). The deconvoluted C1s XPS spectra (Fig. S5) showed four characteristic peaks at 284.6, 285.8, 287.8, and 290.8 eV, which stemmed from C-C, C-OH (or C=N), C-O, and π - π^* respectively. The presence of carbon atoms linked to N or O originated from oxidized PAN precursor containing nitrogen and oxygen. As shown in the summarized functional group ratio obtained from the deconvoluted C1s XPS spectra of the CNSs (Fig. 8a), the ratio of C-C bond increased >55 % in the CNSs carbonized above 1000 °C with considerably reduced carbonyl functional groups. The N1s spectra could be deconvoluted into four peaks consisting of pyridinic N (N-6), pyridonic/pyrrolic N (N-X), quaternary N (N-Q), and oxidized N (N=O) at 398.2, 400.5, 401.1, and 403.1 eV, respectively (Fig. S5).^{40,41} The summarized results of N1s XPS spectra in Fig. 8b illustrate that the reduction of the atomic ratio of N by the higher carbonization temperatures (> 1000 °C) was dominated by the reduction of pyridinic N and pyridonic/pyrrolic N, which is located at the edge of graphene sheets. This result suggests that the connection of C-C networks was facilitated by the breakdown of pyridinic N and pyridonic/pyrrolic N on the edges of neighboring graphitic domains.^{42,43} This result is in agreement with those produced by Raman spectroscopy (Table 1). The quaternary N and oxidized N displays stronger binding energy compared to pyridinic N and pyridonic/pyrrolic N, thus they remained at low concentration in the graphitic domains even after high temperature carbonization, acting as defect sites in the CNSs.

Since the condition for oxidative stabilization for all PAN precursor films was identical, the variation of chemical compositions of CNS-CEs seems to originate from the different temperatures in our catalyst-free carbonization process. Below 1000 °C, the removal

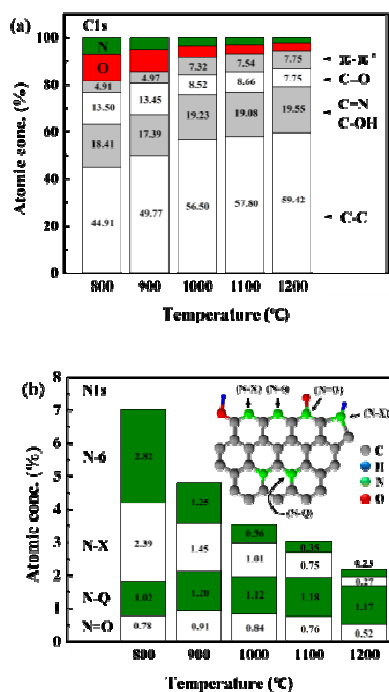


Fig. 8. The composition of functional groups in various CNSs obtained from C1s (a) and N1s (b) XPS spectra. The XPS spectra (wide range and deconvoluted version) of the CNSs are shown in Fig. S5 in SI.

of pyridinic N on the perimeter of graphitic domains was not efficient enough, limiting the merging of neighboring domains, which resists charge conductivity. However, there was no considerable difference in WF and overpotentials for the redox reactions. The presence of heteroatoms in the graphitic domains, especially by N-doping, is known to improve electrical conductivity, electrocatalytic activity, and even electrode/electrolyte interaction.^{41, 44, 45} In our CNSs, however, we could not observe any improvement in terms of electrical conductivity, electrocatalytic activity, and WF locations due to presence of more nitrogen atoms, which actually rather limited the formation of larger graphitic domains. Although the overpotentials for the redox reactions are identical in all CNS-CEs, the enhanced electrical conductivity can improve the chances of electrons reaching the CE/electrolyte interfaces where the electrocatalysis occurs. Since the role of the CEs for DSSCs involves reducing redox couples in the electrolyte for sufficient dye regeneration, the enhanced electrical conductivity can improve the performance of DSSC-CNSs. This is especially true for CNS-CEs that have dual-functions, to act as an electrocatalytic layer and a charge supporting electrode. The electrical conductivity has crucial role in determining the performance of CNS-CEs. Because our CNS electrodes work without FTO, they are good model materials to reveal the relationship between the properties of GBM and their functions as electrodes for electrochemical devices.

Conclusions

Dual-function CNS-CEs for DSSCs were successfully fabricated from a polymeric precursor, PAN, using a catalyst-free carbonization process. The DSSCs using our FTO- and metal-free CE displayed a PCE as high as ~5%. The carbonization conditions determined the amount of residual heteroatoms/functional groups and consequently the size of the resulting graphitic domains. The type of the CNS-CEs considerably influences electrical conductivity, whereas the WF and electrocatalytic activity are similar regardless of the types of CNSs. Since our CNS-CEs were used in the absence of a high-conductivity charge collecting electrode (usually FTO), the electrical conductivity seems to play a crucial role. Our CNSs can be effectively applied as dual-function CEs for DSSCs, and can be used as a good model material for investigating the relationship between the fundamental properties of GBMs and the end-performance as electrodes materials for electrochemical devices.

Acknowledgements

This work was supported by the National Research Foundation (NRF) of Korea grant funded by the Korea government (MEST) (No. 2012045675), the Korea Research Council of Fundamental Science & Technology (KRCF) and KIST for “National Agenda Project (NAP)” program, (SYJ) Global Scholarship Program for Foreign Graduate Students at Kookmin University in Korea (ZAA), and the Korea Institute of Science and Technology Institutional program, Republic of Korea (SL).

Notes and references

- ^a Department of Chemistry, Kookmin University, Seoul 136-702, Korea
^b Carbon Convergence Materials Research Center, Korea Institute of Science and Technology, Wanju, Jeollabuk-do 565-905 Korea
^c Department of Nano Material engineering, University of Science and Technology, Daejeon 305-350, Korea
 *sunghol@kist.re.kr
 †syjang@kookmin.ac.kr
 †Electronic Supplementary Information (ESI) available: Details of the XPS, AFM, and UPS of CNSs. See DOI: 10.1039/b000000x/

- B. Oregan and M. Gratzel, *Nature*, 1991, **353**, 737-740.
- A. Yella, H. W. Lee, H. N. Tsao, C. Y. Yi, A. K. Chandiran, M. K. Nazeeruddin, E. W. G. Diau, C. Y. Yeh, S. M. Zakeeruddin and M. Gratzel, *Science*, 2011, **334**, 629-634.
- T. N. Murakami, S. Ito, Q. Wang, M. K. Nazeeruddin, T. Bessho, I. Cesar, P. Liska, R. Humphry-Baker, P. Comte, P. Pechy and M. Gratzel, *Journal of the Electrochemical Society*, 2006, **153**, A2255-A2261.
- P. Li, J. Wu, J. Lin, M. Huang, Y. Huang and Q. Li, *Solar Energy*, 2009.
- J. Han, H. Kim, D. Y. Kim, S. M. Jo and S. Y. Jang, *ACS Nano*, 2010, **4**, 3503-3509.
- W. Lee, E. Ramasamy and D. Lee..., *ACS applied materials & ...*, 2009.
- J. D. Roy-Mayhew, D. J. Bozym, C. Punckt and I. A. Aksay, *ACS Nano*, 2010, **4**, 6203-6211.

8. S. Y. Jang, Y. G. Kim, D. Y. Kim, H. G. Kim and S. M. Jo, *Acs Applied Materials & Interfaces*, 2012, **4**, 3500-3507.
9. G. Boschloo and A. Hagfeldt, *Accounts of Chemical Research*, 2009, **42**, 1819-1826.
10. S. S. Jeon, C. Kim, T. H. Lee, Y. W. Lee, K. Do, J. Ko and S. S. Im, *Journal of Physical Chemistry C*, 2012, **116**, 22743-22748.
11. K.-C. Huang, C.-W. Hu, C.-Y. Tseng, C.-Y. Liu, M.-H. Yeh, H.-Y. Wei, C.-C. Wang, R. Vittal, C.-W. Chu and K.-C. Ho, *Journal of Materials Chemistry*, 2012, **22**, 14727-14733.
12. X. Xin, M. He, W. Han, J. Jung and Z. Lin, *Angewandte Chemie ...*, 2011.
13. Q. W. Jiang, G. R. Li, S. Liu and X. P. Gao, *The Journal of Physical Chemistry C*, 2010, **114**, 13397-13401.
14. J. M. Kroon, N. J. Bakker, H. J. P. Smit, P. Liska, K. R. Thampi, P. Wang, S. M. Zakeeruddin, M. Gratzel, A. Hinsch, S. Hore, U. Würfel, R. Sastrawan, J. R. Durrant, E. Palomares, H. Pettersson, T. Gruszecki, J. Walter, K. Skupien and G. E. Tulloch, *Progress in Photovoltaics*, 2007, **15**, 1-18.
15. K. S. Lee, H. K. Lee, D. H. Wang, N. G. Park, J. Y. Lee, O. O. Park and J. H. Park, *Chemical Communications*, 2010, **46**, 4505-4507.
16. P. Veerender, S. Vibha, P. Jha, S. P. Koiry, G. Abhay, S. Samanta, A. K. Chauhan, D. K. Aswal and S. K. Gupta, *Organic Electronics*, 2012, **13**.
17. Z. Teng-Long, C. Hong-Yan, S. Cheng-Yong and K. Dai-Bin, *Journal of Materials Chemistry A*, 2013, **1**.
18. J. Chen, B. Li, J. Zheng, J. Zhao, H. Jing and Z. Zhu, *Electrochimica Acta*, 2011.
19. K. Lee, Y. Lee, J. Lee, J.-H. Ahn and J. Park, *ChemSusChem*, 2012, **5**, 379-382.
20. L. Shisheng, L. Yanhong, L. Wei, Y. Wanjing, W. Sida, H. Pengxiang, Y. Quanhong, M. Qingbo, L. Chang and C. Hui-Ming, *Advanced Energy Materials*, 2011, **1**.
21. M. G. Kang, N. G. Park, K. S. Ryu, S. H. Chang and K. J. Kim, *Solar Energy Materials and Solar Cells*, 2006, **90**, 574-581.
22. X. Wang, L. Zhi and K. Müllen, *Nano letters*, 2007, **8**, 323-327.
23. X. Du, I. Skachko, A. Barker and E. Y. Andrei, *Nature nanotechnology*, 2008.
24. S. Bae, H. Kim, Y. Lee, X. Xu, J. S. Park and Y. Zheng..., *Nature ...*, 2010.
25. L. Dan, B. M. Marc, G. Scott, B. K. Richard and G. W. Gordon, *Nature nanotechnology*, 2008.
26. K. V. Emtsev, A. Bostwick, K. Horn, J. Jobst, G. L. Kellogg, L. Ley, J. L. McChesney, T. Ohta, S. A. Reshanov and J. Röhrl, *Nature materials*, 2009, **8**, 203-207.
27. A. C. Ferrari and J. Robertson, *Physical Review B*, 2000, **61**, 14095-14107.
28. G. Srinivas, Y. W. Zhu, R. Piner, N. Skipper, M. Ellerby and R. Ruoff, *Carbon*, 2010, **48**, 630-635.
29. A. C. Ferrari and J. Robertson, *Physical Review B*, 2001, **64**, 075414.
30. D. S. Knight and W. B. White, *Journal of Materials Research*, 1989, **4**, 385-393.
31. F. Fabregat-Santiago, J. Bisquert, G. Garcia-Belmonte, G. Boschloo and A. Hagfeldt, *Solar Energy Materials and Solar Cells*, 2005, **87**, 117-131.
32. H.-J. Ahn, I.-H. Kim, J.-C. Yoon, S.-I. Kim and J.-H. Jang, *Chemical Communications*, 2014, **50**, 2412.
33. V.-D. Dao, N. T. Q. Hoa, L. L. Larina, J.-K. Lee and H.-S. Choi, *Nanoscale*, 2013, **5**, 12237.
34. H. Jeong, Y. Pak, Y. Hwang, H. Song, K. H. Lee, H. C. Ko and G. Y. Jung, *Small*, 2012, **8**, 3757-3761.
35. F. Fabregat-Santiago, J. Bisquert, E. Palomares, L. Otero, D. Kuang, S. M. Zakeeruddin and M. Gratzel, *Journal of Physical Chemistry C*, 2007, **111**.
36. S. M. Park and J. S. Yoo, *Analytical Chemistry*, 2003, **75**, 455a-461a.
37. A. I. Popov and D. H. Geske, *Journal of the American Chemical Society*, 1958, **80**, 1340-1352.
38. Y. G. Kim, Z. A. Akbar, D. Y. Kim, S. M. Jo and S. Y. Jang, *Acs Applied Materials & Interfaces*, 2013, **5**, 2053-2061.
39. S. Das, P. Sudhagar, E. Ito, D. Y. Lee, S. Nagarajan, S. Y. Lee, Y. S. Kang and W. Choi, *Journal of Materials Chemistry*, 2012, **22**, 20490-20497.
40. H. Wang, T. Maiyalagan and X. Wang, *ACS Catalysis*, 2012, **2**, 781-794.
41. Z.-S. Wu, S. Yang, Y. Sun, K. Parvez, X. Feng and K. Müllen, *Journal of the American Chemical Society*, 2012, **134**, 9082-9085.
42. W. Watt, *Nature physical science* 1972, **236**, 10-11.
43. M. S. A. Rahaman, A. F. Ismail and A. Mustafa, *Polymer Degradation and Stability*, 2007, **92**, 1421-1432.
44. Y. Xue, J. Liu, H. Chen, R. Wang, D. Li, J. Qu and L. Dai, *Angewandte Chemie International Edition*, 2012, **51**, 12124-12127.
45. Z.-S. Wu, A. Winter, L. Chen, Y. Sun, A. Turchanin, X. Feng and K. Müllen, *Advanced Materials*, 2012, **24**, 5130-5135.